Order N^o : ../../..

PEOPLE'S DEMOCRATIC REPUBLIC OF ALGERIA
MINISTRY OF HIGHER EDUCATION AND SCIENTIFIC RESEARCH
UNIVERSITY KASDI MERBAH OF OUARGLA

Faculty of New Information Technologies and Communication
Department of Electronics and Telecommunications

ACADEMIC MASTER'S DEGREE

Field : **Sciences and Technology**

Branch : **Telecommunications**

Option : **Systems of Telecommunications**

presented By :

Sarhani Khalil

Yahiouche Amor

Theme

A comparative study between handcrafted features and deep features for biometric systems

Publicly defended on 03/06/2025 before the jury composed of :

KORICHI Maarouf	*MCA*	*University Kasdi Merbah - Ouargla*	*President*
SAMAI Djamel	*Pr.*	*University Kasdi Merbah - Ouargla*	*Supervisor*
MEBARKIA Mariem	*MAB*	*University Kasdi Merbah - Ouargla*	*Examiner*

Dedication

I dedicate this significant event in my life to :

My parents, who have been my steadfast supporters and the guiding lights of my life. My dear brother and sisters, whose unwavering belief and support have been invaluable.
To my colleague yahiouche Amor I wish him a bright and happy future.and my friends and all the acquaintances I met during my university studies.
My professor, for believing in me and providing the support and guidance needed to write this productive and enjoyable thesis.

Sarhani khalil

Dedication

With sincere gratitude and admiration, I dedicate this modest work :

My parents, who have been my steadfast supporters and the guiding lights of my life. My dear brother and sisters, whose unwavering belief and support have been invaluable.
To my colleague Sarhani Khalil I wish him a bright and happy future.and my friends and all the acquaintances I met during my university studies.
My professor, for believing in me and providing the support and guidance needed to write this productive and enjoyable thesis.

Yahiouche Amor.

Acknowledgments

First, we thank God (ALLAH) for giving us patience and courage. We extend our sincere thanks to Professor Djamel SAMAI, who supervised This project has provided valuable advice and basic guidance. We sincerely appreciate his patience, the efforts he has shown, and their significant contributions to the development of this research. His support was instrumental in achieving the positive results of our study. We would also like to thank the jury members. Dr. KORICHI Maarouf and Dr. MEBARKIA Mariem for agreeing to review and evaluate our study. We also take this opportunity to express our sincere thanks to all teachers for their collaboration, presence, and empathy throughout our education.

To all my colleagues and friends——thank you so much.

الملخص

تُعنى القياسات الحيوية بتحديد هوية الأفراد اعتمادًا على خصائصهم الفسيولوجية أو السلوكية. وتُعد الأنظمة البيومترية من الأدوات الأساسية في العديد من التطبيقات الأمنية. تهدف هذه المذكرة إلى دراسة مقارنة بين منهجين لاستخراج السمات البيومترية : السمات المصممة يدويًا(Handcrafted) مثل LPQ ML-LPQ ، والسمات العميقة(Deep Features) المستخرجة باستخدام الشبكات العصبية العميقة مثل AlexNet و DenseNet-201 . تم استخدام صور كف اليد كنموذج للبيانات البيومترية، وتم تقييم أداء كل منهج من حيث الدقة، سرعة المعالجة، والتعقيد الحسابي. أظهرت النتائج أن السمات العميقة توفر دقة أعلى، بينما تتميز الطرق اليدوية ببساطة التنفيذ. تقترح هذه الدراسة إمكانية الدمج بين الطريقتين لتحقيق أداء متوازن وفعّال

الكلمات المفتاحية السمات اليدوية كف اليد التعلم العميق، القياسات الحيوية ، التعلم المنقول، أحادي الوضع، متعدد الوضع.

Abstract

Biometrics involves identifying individuals based on their physiological or behavioral traits. Biometric systems are essential tools in many security-related applications. This dissertation compares two feature extraction approaches : handcrafted methods such as LPQ and ML-LPQ and deep learning-based methods using neural networks like AlexNet and DenseNet-201. Palmprint images were used as the biometric data source. The evaluation focused on accuracy, processing speed, and computational complexity. The results show that deep features offer higher accuracy, while handcrafted methods are simpler and faster. Combining both approaches can lead to more balanced and effective biometric systems.

Keywords : Biometrics, palmprint, handcrafted features, deep features.

Contents

List of Figures

Abbreviations

AI :	Artificial Intelligence
CMC :	Cumulative Match Characteristic
CNN :	Convolution Neural Network
DL :	Deep Learning
EER :	Equal Error Rate
FAR :	False Accept Rate
FKP :	Finger Knuckle Print
FRR :	False Reject Rate
GAR :	Genuine Acceptance Rate
ML :	Machine Learning
ReLU :	Rectifed Linear Unit
ROC :	Receiver Operating Characteristic
ROR :	Rank One Recognition
RPR :	Rank of Perfect Recognition
SUM :	Summation
WSUM :	weighted sum
SVM :	Support Vector Machine
T0 :	Threshold

Chapter 1

General introduction

Within the time of fast advanced change, the requirement for secure and effective character confirmation strategies is more basic than ever. Biometric frameworks have developed as a strong arrangement by utilizing special physiological and behavioral characteristics such as fingerprints, facial highlights, iris designs, and voice signals for exact individual distinguishing proof. Unlike conventional verification strategies (e.g., passwords or ID cards), biometrics offer inherent resistance to theft, duplication, and impersonation.

The feature extraction process is a vital component in any biometric framework, which changes crude biometric information into a compact and discriminative representation. Historically, this task has been accomplished using handcrafted features, which are designed based on expert knowledge in image processing, signal analysis, or pattern recognition. Local Binary Pattern (LBP) and Local Phase Quantization (LPQ) drop beneath this category. These strategies are computationally productive and interpretable but regularly battle to preserve vigor beneath shifting conditions such as lighting, posture, or noise.

In contrast, the rise of deep learning introduced expression-deep properties that automatically learn from data using deep neuronal networks, particularly convolutional neural networks (CNNs). These models can capture complex and abstract patterns without manual design and perform excellently in many challenging biometric scenarios. Deep features show high tuning and generalization functions, especially when trained on large

data records.

This study compares handcrafted and deep features in biometric recognition systems and assesses their performance across numerous biometric modalities and operational scenarios. The objective is to understand the benefits, limits, and applicability of each technique and give insights into how current advances in deep learning are transforming the field of biometrics.

This dissertation is organized as follows.

The first chapter gives a general introduction to the work done.

The second chapter describes the basic ideas of biometrics, including properties, criteria, and classifications. It also discusses the process involved in biometric identification systems and presents the architecture of the multimodal biometric identification system. This chapter concludes with performance assessments for biometric systems.

The third chapter delves into the concepts of handcraft and deep learning methods. The last is based on transfer learning and focuses on the bypass neural networks (CNN) used to derive deep features. To evaluate the effectiveness and accuracy of the biometric recognition systems, these deep features extracted from networks such as AlexNet and DenseNet201 were compared to handcrafted features such as LPQ and ML-LPQ.

The fourth chapter includes experiments to compare the performance of handcraft methods (LPQ and ML-LPQ) of biometric systems based on palmprint and deep learning methods based on transfer learning (AlexNet and DenseNet201 networks). Each method was evaluated using SVM classifiers and metrics such as EER, GAR, and ROR. The results showed deep learning methods perform better than handcrafted methods, especially in AlexNet networks. Integrating modalities (multimodal fusion) also contributed to improving the system's overall performance.

The fifth chapter presents the general conclusion and future work. It summarizes the most important research findings and provides recommendations for additional research.

Chapter 2

Basics of Biometrics

2.1 Introduction

The demand for effective identification and authentication has reached new heights in today's quickly changing technological world and rising reliance on digital information. In this environment, biometric identification systems are an important tool across several sectors. Throughout this chapter, we explored durable biometric attributes like fingerprints, facial features, or iris scans, which identify and verify individuals' identities, offering more accuracy and security than older approaches based on passwords or smart cards. Biometric identity technologies have a distinct benefit in that an individual's biometric data cannot be easily reproduced or fabricated, making them more dependable when working with security systems and computers. In this chapter, we will look into biometric identification systems in further detail, including their design, assessment, and applications in security, surveillance, and digital identity management.

2.2 Definition of biometrics

Biometrics is a technique for identifying and verifying people by turning their biological, physical, or behavioral characteristics into digital data. Its purpose is to determine a person's identity based on fixed aspects of their anatomy or behavior. Biometric authentication uses physiological traits or behavioral patterns to identify and recognize individuals. [1]. Physiological traits include the iris, fingerprint, palm print, hand geometry, and facial features. Meanwhile, behavioral qualities include voice, signature, and

movement, among others, as illustrated in (Figure 2.1).

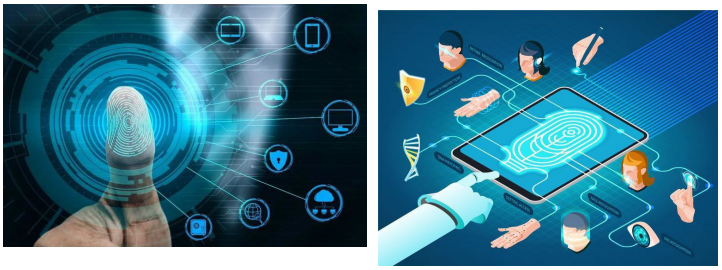

Figure 2.1 – Some biometric modalities

2.3 Biometrics classifications

Different biometric modalities are utilized in various areas, and we may identify three categories (Figure 2.2).

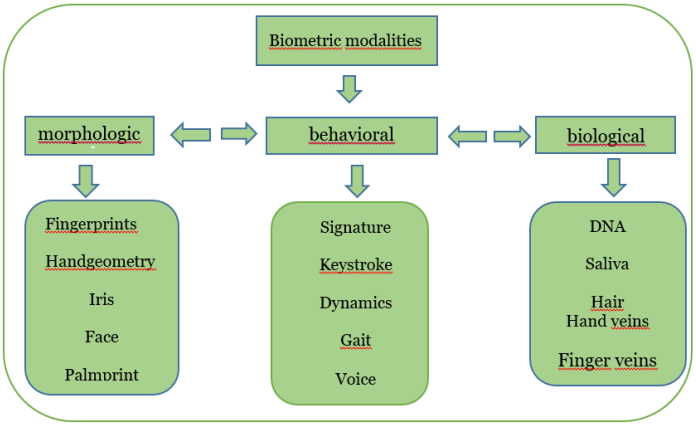

Figure 2.2 – Categorization of various biometric modalities

2.3.1 Physical characteristics

They are interested in anything related to the external appearance of the various organs, including the following:

2.3.1.1 Finger Knuckle Print (FKP)

The Finger Knuckle Print (FKP) refers to the distinct patterns created by the ridges and grooves on the skin that cover the finger joints. Unlike regular fingerprints, FKP is often regarded as more trustworthy. A sensor collects these prints and compares them with a database for identification and verification. FKPs are commonly used in security systems to protect financial transactions and access to critical facilities [2] (Figure 2.3).

Figure 2.3 – Biometric system based on finger knuckles print

2.3.1.2 Fingerprint

The most often used biometric technology is fingerprint identification. This is the oldest biometric technology [3] (Figure 2.4).

Figure 2.4 – images of fingerprint

2.3.1.3 Palmprint

The palmprint is the region between the wrist and the fingers, and it contains characteristics such as principal lines, wrinkles, ridges, minutiae points, single points, and texture patterns that can be recovered from a low-resolution photograph. Since the palm is significantly larger than a finger, researchers predict that palmprints will be more distinct than fingerprints or even finger knuckle prints. Among biometric modalities, palmprint has attracted much interest from researchers as a novel biometric recognition method [4] (Figure 2.5).

Figure 2.5 – Images of palm print

2.3.1.4 Iris

The iris is the colorful eye area that surrounds the black pupil. A camera captures the iris to adjust for the pupil's natural movements. Its comprehensive examination shows numerous unique and independent intricate structures dates of the individual's genetic code, which do not fluctuate over life [5] (Figure 2.6).

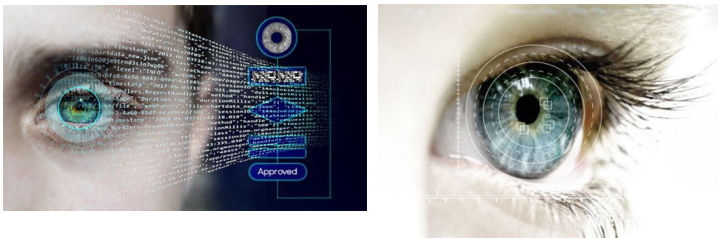

Figure 2.6 – images of fingerprint

2.3.1.5 Face

Face recognition is humans' most prevalent biometric feature for achieving personal identification. Face recognition relies on the form and placement of the eyes, brows, nose, lips, and chin, as well as an overall analysis of the face picture, which portrays a face as a collection of known faces. Matching face photos obtained from various angles and under varying lighting circumstances is difficult in a face recognition system. Furthermore, the face of an individual might vary with time. These factors make face recognition systems dubious whether the face alone can distinguish a person from many identities [6] (Figure 2.7).

Figure 2.7 – Face recognition

2.3.1.6 Hand geometry

Hand geometry is the longest-used biometric, first appearing in the market in the late 1980s. The systems are extensively used because of their simplicity, public acceptability, and integration possibilities. The gadgets work on the simple principle of measuring and recording a person's hand's length, breadth, thickness, and surface area as it is moved across a plate. However, this biometric can change over time [7] (Figure 2.8).

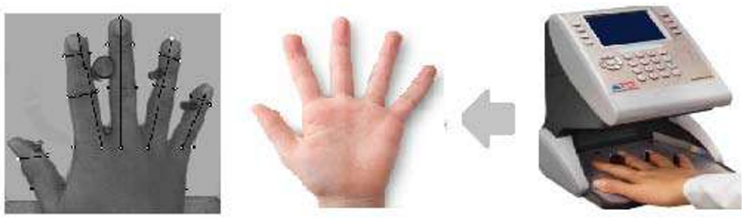

Figure 2.8 – images of Hand geometry

2.3.2 Behavioral characteristics

This category focuses on evaluating an individual's behavior.

2.3.2.1 Keystrokes

Keystroke dynamics is studying how a person types on a peripheral device by monitoring keyboard inputs hundreds of times per second to identify users based on their typical typing rhythm patterns. It has already been demonstrated that keyboard rhythm is a reliable identification indicator. Furthermore, unlike other biometric systems, which can be costly to construct, keystroke dynamics is nearly free; the only hardware required is a keyboard [8] (Figure 2.9).

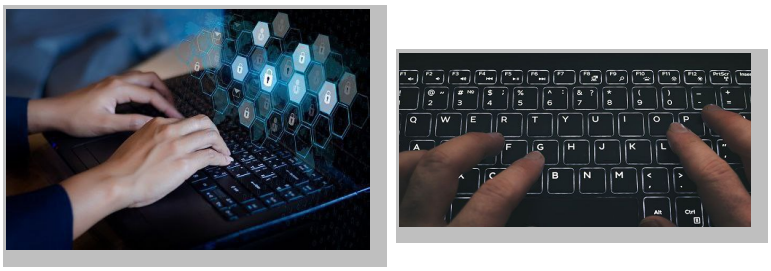

Figure 2.9 – Typing image

2.3.2.2 Voice

Voice biometrics confirms a person's identification by analyzing the peculiarities of their voice. Real-world security applications have been using these systems for over a decade. Their application is quickly rising across a wide range of businesses, including financial services, retail, maintenance, and even entertainment [9] (Figure 2.10).

Figure 2.10 – voice recognition image

2.3.2.3 Signature

A signature is described as a person's method of signing his or her name, which is recognized as a trait of that individual. Signature-based recognition systems may be used in two ways: static mode, in which users write their signature on paper and digitize it using an optical scanner or camera, and the biometric system, which detects the signature by analyzing its structure. This group is often referred to as "off-line". The second option is Dynamic. In this mode, users write their signature on a digitized tablet, which captures it in real time. Some systems also work on smartphones or tablets with capacitive screens, allowing users to sign with a finger or the proper pen. "On-line" is another term for dynamic recognition. Dynamic information often includes geographical coordinates (x(t), y(t)), pressure, azimuth, inclination, and pen up/down. This technology has been primarily focused on e-business applications and other applications where signatures are accepted as a form of personal authentication [10] (Figure 2.11).

2.3.2.4 Gait

Gait recognition is an area of biometrics that, unlike other biometrics, is unobtrusive since it does not use body-invasive sensors to acquire gait information. Gait recognition is an appealing surveillance modality since it may be carried out remotely and covertly. Most

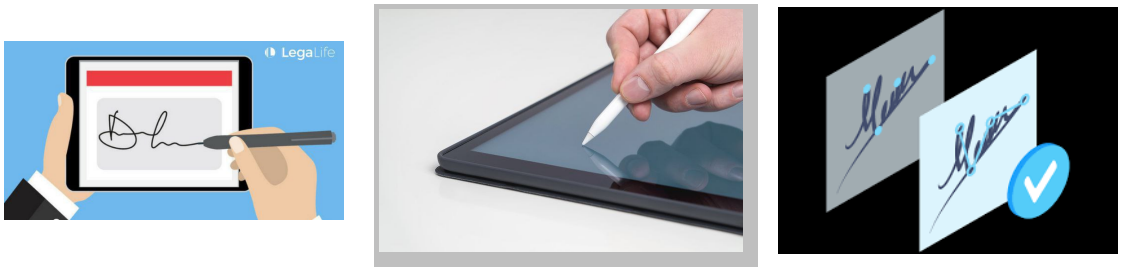

Figure 2.11 – Signature images

other modalities need proximate sensing, making them challenging for many people to deploy in an unobserved setting. Furthermore, humans can recognize individuals even from poor-quality gait demonstrations, the availability of identifying information (Figure 2.12).

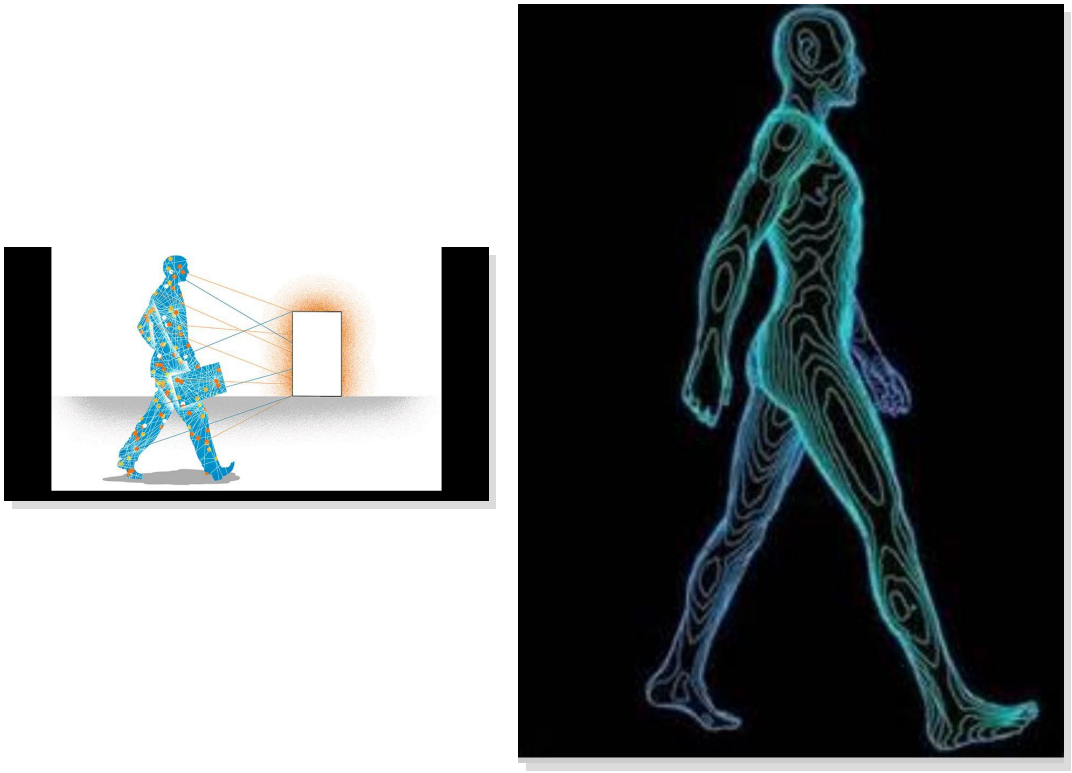

Figure 2.12 – Images of gait system

2.3.3 Biological characteristics

This biometric modality, which incorporates unique traits such as DNA, saliva, and odor, provides a solid foundation for exact individual identification.

2.3.3.1 DNA

DNA sampling is currently invasive, requiring the collection of tissue, blood, or other body samples. This capture method still needs refinement. DNA analysis has not

yet been automated enough to qualify as a biometric technique. Human DNA analysis is now feasible in as little as 10 minutes. As technology evolves such that DNA can be automatically changed in real time, it can become more significant at the moment [11] [12] (Figure 2.13).

Figure 2.13 – DNA images

2.4 Biometrics Systems Applications

Various industries are rapidly using biometric technologies to identify and authenticate individuals based on their unique biological traits. Here are the primary applications.

- **Enforcement and Public Security:** Biometrics are important for criminal identification, with systems such as Automated Fingerprint Identification Systems (AFIS) used to compare fingerprints and facial recognition technology utilized in surveillance.
- **Military:** Biometrics are used to identify allies and opponents, improving security in military operations.
- **Border and Immigration Control:** Biometric devices improve passenger identification at borders, increasing security and efficiency in immigration operations.
- **Civil Identification:** Governments use biometrics for voter registration and national ID systems, which ensure correct citizen identity.
- **Healthcare:** Biometrics help identify patients and healthcare professionals, facilitate access to medical treatments, and decrease fraud in healthcare benefits.
- **Access Control:** Biometrics safeguard entrance in both physical (building access) and logical (digital device access) systems, frequently replacing traditional passwords with

fingerprint or face recognition.

• **Mobile Applications:** Today's mobile devices frequently employ biometric authentication technologies like fingerprint scanning and face recognition for app security and transactions, boosting user convenience while ensuring security.

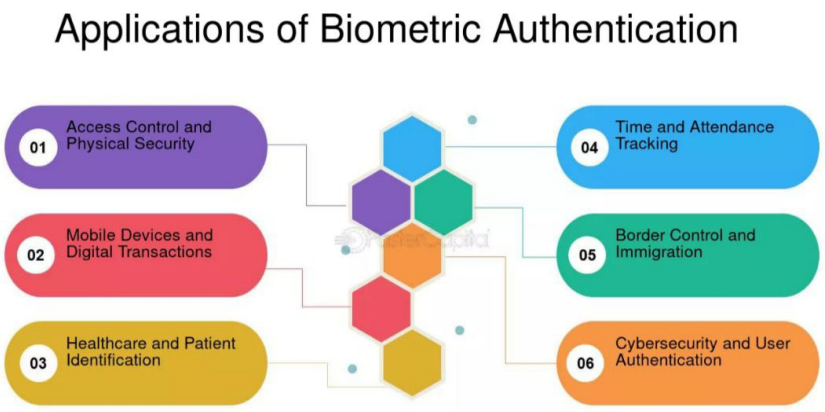

Figure 2.14 – Biometrics Systems Applications

2.5 Operating modes of a biometric system

Biometric systems are technical systems that use information about a person's biometric features to identify or verify that person. Looking at biometric systems broadly reveals several commonalities among biometric-based authentication systems. In general, such systems operate in two stages.

2.5.1 Enrollment

This method collects biometric user data. Biometric scanners are typically used for this purpose. Subsequently, the collected data is kept in a central database and tagged with a user identity (such as name or identification number) to make identification easier [13] (Figure 2.15).

2.5.2 Verification

The system compares the claimed identity with the stored one in verification mode, a one-to-one $(1:1)$ matching procedure. If the claimed identity's matching score exceeds a predetermined threshold$\alpha \in (0,1)$, the claimed identity is acknowledged as authentic; if not, it is rejected as an impostor. Therefore, the authentication process might be

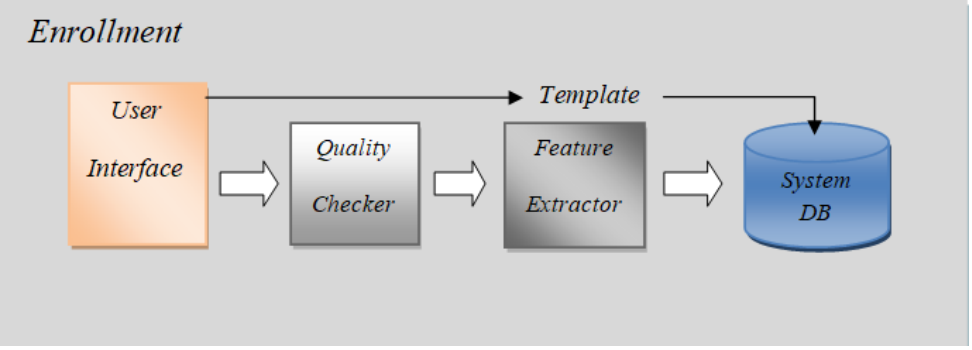

Figure 2.15 – mode Enrollment

implemented as a binary classification problem and run according to the verification mode [14] (Figure 2.16).

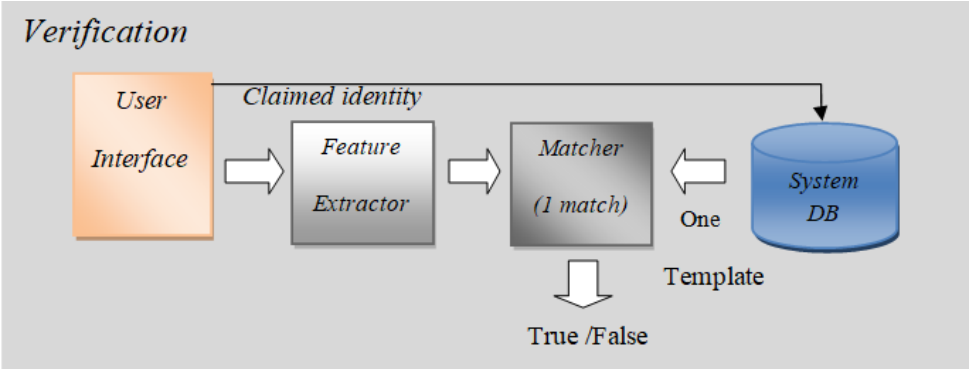

Figure 2.16 – mode Verification

2.5.3 Identification

The system identifies the biometric sample in identification mode, which is a one-to-many $(1:N)$ matching process, by comparing it with all stored templates (i.e., a template for each user). The matching stage then determines the user identity based on the highest matching score and a predetermined threshold (i.e., multiple matching scores will be generated, one for each user, in which the highest score will be selected). Let's look at VU, the biometric information that the system gathers when a user U is in front of it. Therefore, identification entails figuring out who $I_i, i \in [0,1,2,...,N]$, where I_0 is an unknown identity, and $I_1, I_2, ..., I_N$ are user identities that have already been enrolled in the system [15] (Figure 2.17).

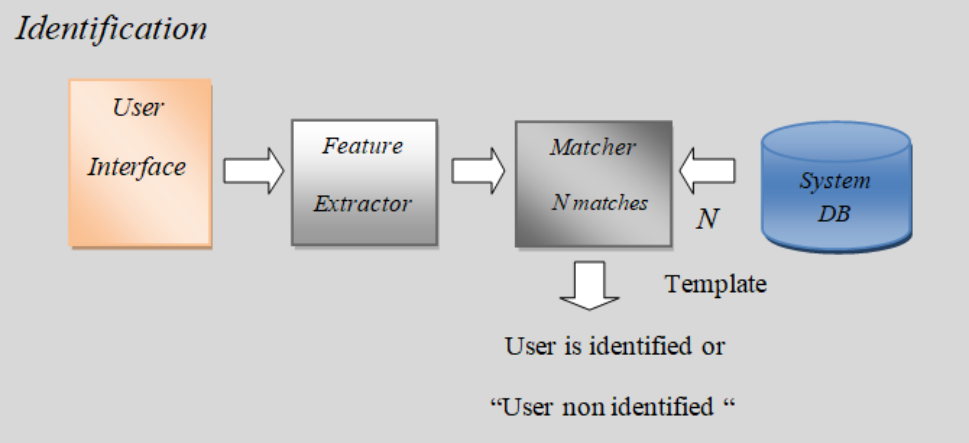

Figure 2.17 – mode Identification

2.6 Evaluation of biometric systems

A biometric system's performance is examined in order to assess its reliability and quality. When evaluating a biometric system, important considerations include.

2.6.1 False Rejection Rate (FRR)

The False Rejection Rate measures the probability that the biometric system mistakenly rejects an authorized user. Regarding biometric authentication, the FRR is the rate at which the system does not recognize a valid user, resulting in a false rejection. [16]. One method of calculating FRR is to use the following formula, where NC is the number of customers in the database and FR(T) is the False Rejection rate, which indicates the frequency of false rejections.

$$FRR = \frac{\text{Total number of False Rejections}}{\text{Total number of 'Genuine' Attempts}} \tag{2.1}$$

2.6.2 False Acceptance Rate (FAR)

The False Acceptance Rate measures the probability that the biometric system may mistakenly accept an illegal user. The FAR is the rate at which the system misidentifies an unauthorized user as genuine, resulting in a false positive in biometric authentication. [16]. Completing the FAR computation involves the following:

$$FAR = \frac{\text{Total number of False Acceptances}}{\text{Total number of 'Imposter' Attempts}} \tag{2.2}$$

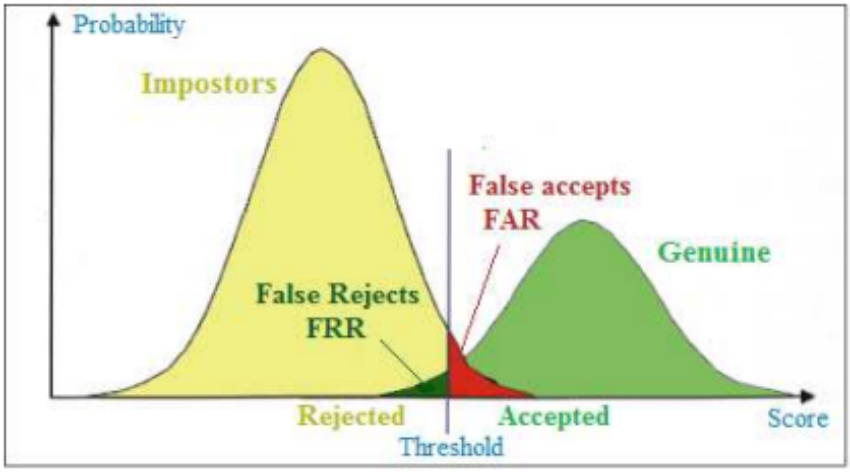

Figure 2.18 – FAR and FRR diagrams

Figure 2.18 displays the FAR and FRR diagrams based on the distributions of real and fake scores.

2.6.3 DET(Detection Error Trade)

The Detection Error Trade-off (DET) curve in a biometric system shows how the False Acceptance Rate (FAR) and the False Rejection Rate (FRR) are. The plot is done parametrically using the threshold [17].

2.6.4 ERR (Equal Error Rate)

The Equal Error Rate (EER) is the third requirement. The moment at which the False Acceptance Rate (FAR) and the False Rejection Rate (FRR) are equal is known as the Equal Error Rate (EER). Another name for this rate is the crossover error rate. It is an essential standard for assessing a biometric system's overall performance [16].

2.6.5 Receiver Operating Characteristics Curve (ROC)

The Receiver Operating Characteristic (ROC) curve provides a graphical representation of the trade-off between the False Acceptance Rate (FAR) and the False Rejection Rate (FRR) at various operating points, making it widely used to assess the performance of biometric systems [18] (Figure 2.19).

2.6.6 Cumulative Matching characteristic Curve (CMC)

The Cumulative Match Characteristic (CMC) curve is a commonly used indicator to assess the effectiveness of biometric identification systems. It gives a visual represen-

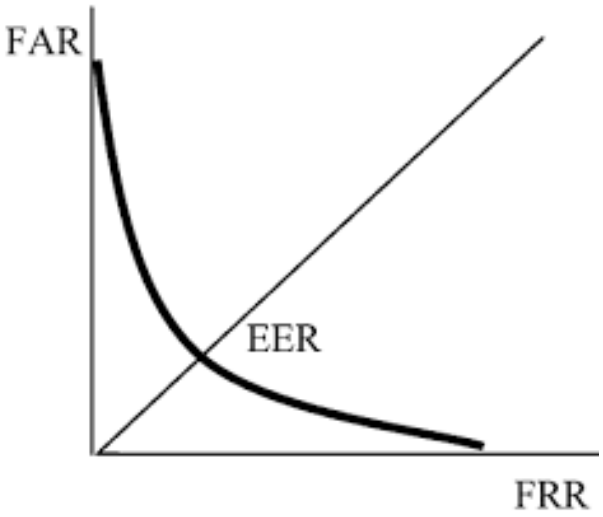

Figure 2.19 – ROC curve

tation of how well the algorithm finds people in the top rankings of a list of candidates [19] (Figure 2.20).

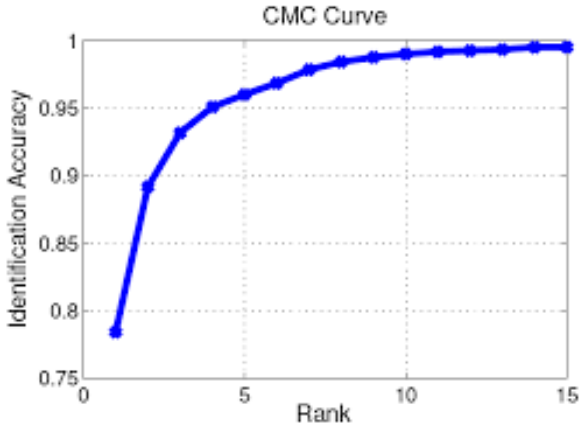

Figure 2.20 – CMC curve

2.7 Conclusion

In this chapter, we discussed the concept of biometric systems, their design, and several uses. Several factors influence the performance of biometric systems, which varies from system to system. We provided equal error rates as criteria for assessing the biometric system's quality.

Chapter 3

Handcrafted features and deep features for biometrics

3.1 Introduction

Biometric systems play a vital role in artificial intelligence and information security by offering reliable methods for identity verification based on physical or behavioral traits. A key factor in their effectiveness is the ability to extract distinctive features for accurate recognition. Feature extraction techniques have evolved into two main categories: **handcrafted features**, which rely on manually designed algorithms, and **deep features**, which are automatically learned using deep neural networks. This chapter introduces the core concepts of biometric systems, focusing on these two types of features and their importance in building robust systems. Common applications in face, fingerprint, and iris recognition will also be explored.

3.2 Handcrafted Features

Handcrafted features in biometric systems refer to features or characteristics that are designed and extracted manually from raw biometric data using specific techniques and algorithms. The goal of these features is to represent the data in a way that makes it usable for classification or verification processes. This is done by extracting unique and distinctive information from the data, such as geometric or statistical patterns. Hand-

crafted features rely on human knowledge and experience in choosing relevant traits that can distinguish between individuals. For example, in fingerprints, details such as branching points (minutiae) and intersections are extracted. In facial recognition, the focus is on facial features such as the distances between the eyes or the shape of the jaw. In voice biometrics, frequencies and tones are analyzed. These features are hand-crafted based on a deep understanding of biometric characteristics. There are many types that are used in manual features to derive characteristic features from photos and biometric data. Among these features, we find Local Binary Patterns (LBP) and Local Phase Quantization (LPQ).

3.2.1 Local Binary Pattern Method (LBP)

The Local Binary Pattern (LBP) operator was first proposed by Ojala et al. [20]. in order to characterize the texture of a picture. The LBP value is calculated for each pixel by summing its eight immediate neighbors with a threshold. The approach has now been expanded to include different-sized neighbors. All neighbors will be assigned a value of 1 if their value is greater than or equal to the current pixel and 0 otherwise. The LBP code for the current pixel is generated by concatenating 8 values into a binary code. As in a grayscale image, the LBP values are represented as pixels with intensities ranging from 0 to 255.

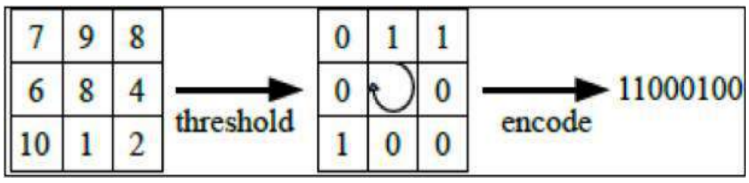

Figure 3.1 – LBP operator

In this case, a radius R circle is drawn around the central pixel, and the values of the P points on its edge are measured and compared to the central pixel's value. An interpolation is required to obtain the values of the P points sampled in the neighborhood for each R-ray. To define the neighborhood of P points with radius R of a pixel, the notation (P, R) is used. depicts three neighborhoods with varying R and P values [21] [22].

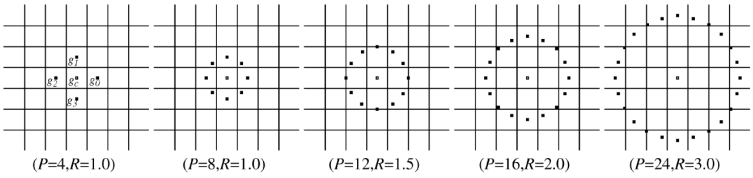

Figure 3.2 – Three neighborhoods for different R and P.

3.2.2 Local Phase Quantification (LPQ)

The Local Phase Quantization (*LPQ*) was first proposed by Ojansivu and Heikkilä for texture description [23]. The descriptor *LPQ* utilizes local phase information obtained from a short-term Fourier transform (*STFT*) applied over a rectangular M-by-M neighborhood N_x at each pixel position x of the image $f(x)$, as defined below:

$$F(u,x) = \sum_{y \in N_x} f(x-y) e^{-j2\pi u^T y} = W_u^T f_x \tag{3.1}$$

Where W_u is the basis vector of $2-D$ DFT at frequency u, and f_x is the vector containing all M^2 samples from N_x.
The equation is efficiently evaluated for all image positions $x \in \{x_1, x_2, \ldots, x_N\}$ using 1-D convolutions for rows and columns successively.

The LPQ feature is extracted from a local region in the *FFT* domain. According to [24], the local Fourier coefficients for each pixel are calculated at four specific frequency points: $u_1 = [a,0]^T$, $u_2 = [0,a]^T$, $u_3 = [a,a]^T$, and $u_4 = [a,-a]^T$, where a is the frequency parameter.

For each pixel position, these coefficients create a vector $F_x = [F(u_1,x), F(u_2,x), F(u_3,x), F(u_4,x)]$. The phase information in the Fourier coefficients is captured by examining the signs of the real and imaginary parts of each component in F_x. This is achieved through a simple scalar quantizer.

Next, to retrieve the phase information for each pixel in the specified neighborhood, a binary scalar quantizer is applied to quantify the signs of the real and imaginary parts of each coefficient. Finally, the quantization results for each coefficient are encoded into an 8-bit binary string.

$$q_j = \begin{cases} 1 & if\ q_j \geq 0 \\ 0 & otherwise \end{cases} \tag{3.2}$$

Where $q_j(x)$ is the j^{th} component of the vector $G_x = [ReF_x, ImF_x]$. The resulting eight-bit binary coefficients $q_j(x)$ are represented as integers by using binary coding:

$$f_{LPQ(x)} = \sum_{j=1}^{8} q_j 2^{j-1} \tag{3.3}$$

By analyzing the values from each image pixel, we can create a histogram represented as a vector of 256 features. Figure 1 illustrates how to compute this descriptor [21].

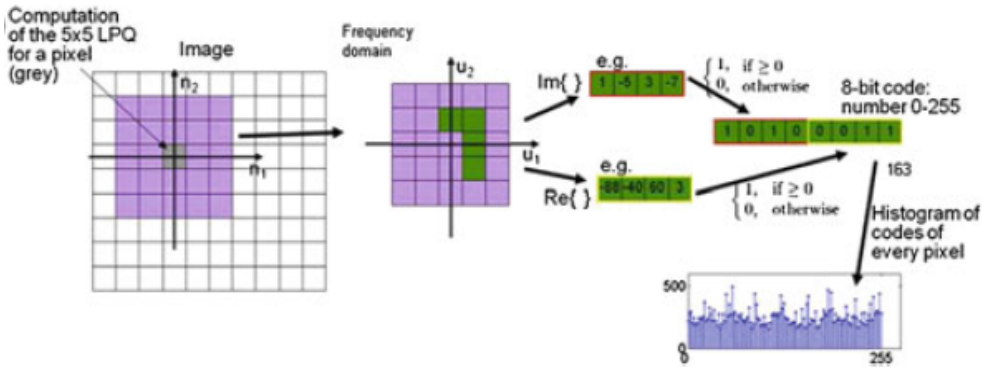

Figure 3.3 – Example of computation of the *LPQ* descriptor

3.2.3 Multi-Level of Local Phase Quantization

Multi-Level Local Phase Quantization enhances the original LPQ algorithm. This approach divides the image into sub-blocks and applies the LPQ algorithm at different levels. For example, if we want to calculate the LPQ at three levels, we start by setting the LPQ descriptor for the entire image at level 1. At level 2, we divide the image into two equal sub-blocks and apply the LPQ descriptor to each sub-block. For level 3, we further split the image into three sub-blocks and again applied the LPQ descriptor to each. We generate 1 histogram from level 1, 4 histograms from level 2, and 9 histograms from level 3. We get $1^2 + 2^2 + 3^2 = 14$ histograms, which we then combine into a single feature histogram.

3.3 DEEP LEARNING

Biometric systems often utilize deep learning methodologies that stack numerous layers of algorithms. Biometric systems employ a supervised learning technique for identification. Deep learning is not dependent on a particular method or strategy; rather, it is a

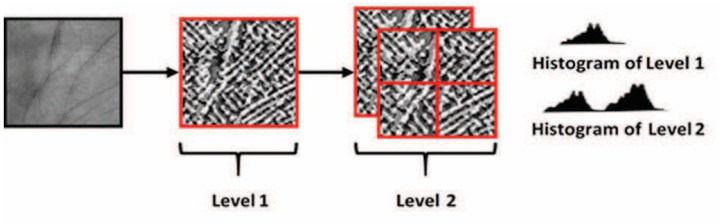

Figure 3.4 – Representation of 2 levels of ML-LPQ

collection of methods and topologies that are used to tackle a range of problems. What distinguishes deep learning is its progressive nature. It emphasizes the collection of successive layers of more relevant representations from the available data. A deep learning model learns from the data at each layer, passing information from one layer to the next. This approach is similar to how lower layers in image processing may distinguish borders, while higher levels may recognize notions that are essential to people, such as faces, letters, or numbers [25].

Deep neural networks are complex artificial neural networks with several hidden layers between the input and output layers [26].

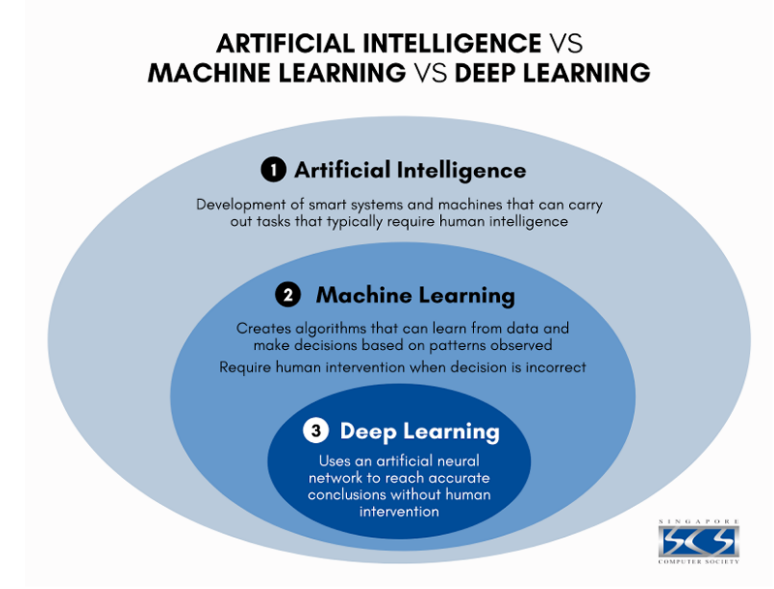

Figure 3.5 – DEEP LEARNING

3.3.1 Deep Learning Types

Depending on the type of learning process, deep learning algorithms can be categorized into the following:

3.3.1.1 Supervised learning

Supervised learning relies on a training dataset containing examples for both inputs and labeled output values. These input-output pairs are used to adjust the parameters of the machine-learning model. Once trained, the model can predict the target variable for new input data. Supervised learning can be categorized into regression problems, where numeric values are predicted, and classification problems, where the prediction is a categorical class.

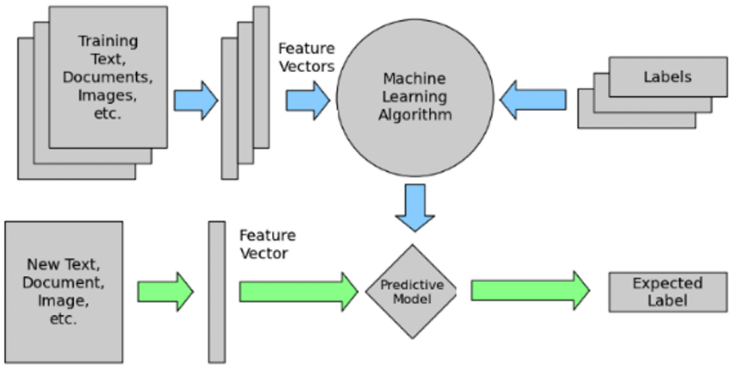

Figure 3.6 – Supervised learning Model

3.3.1.2 Unsupervised Learning

Unsupervised learning occurs when a system learns to identify patterns without predefined labels. In this type of learning, the training data consists solely of input variables x, aiming to uncover structural information, such as identifying groups of elements with shared characteristics or reducing the dimensionality of the data by projecting it into a lower-dimensional space (dimensionality reduction).

3.3.1.3 Semi-supervised learning:

Semi-supervised learning is a class of supervised learning tasks and techniques that leverage both labeled and unlabeled data for training. Typically, only a small portion of the data is labeled, while the majority remains unlabeled. This approach bridges the

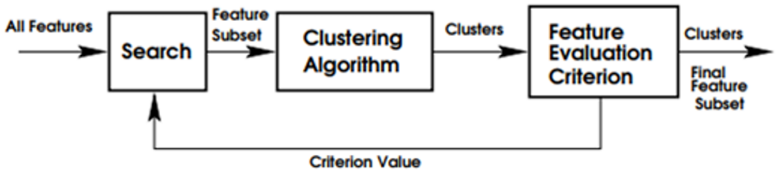

Figure 3.7 – Example approach for unsupervised learning

gap between unsupervised learning, which lacks labeled data altogether, and supervised learning, which relies entirely on labeled data. Researchers have discovered that incorporating unlabeled data alongside a limited amount of labeled data can significantly enhance learning accuracy.

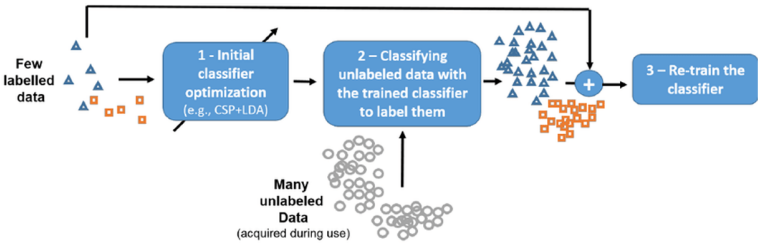

Figure 3.8 – Principle of semi-supervised learning.

3.3.2 Deep Learning models

Deep learning methods are fast evolving to provide higher performance. The literature includes adequate review papers on the progressing algorithms of deep learning in particular application domains. The family of deep learning methods has been growing increasingly richer, including models of neural networks. In this section, we present the most important and most popular models in the field of deep learning.

3.3.2.1 Deep Neural Network (DNN)

DNN is a neural network that integrates a specific level of complexity, which means that several hidden layers are placed between the input and output layers [27]. A deep neural network (DNN) consists of several hidden layers. This architecture aims to create an abstract representation or high-level model of observation data. This is then used to identify highly nonlinear mappings between input data and target values. DNNs have a long history of development. The figure shows an example of picture classification.

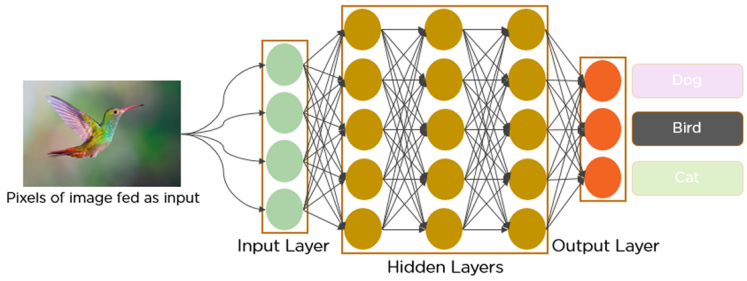

Figure 3.9 – Example of classification by Deep Neural Network (DNN)

3.3.2.2 Restricted Boltzmann Machine (RBM)

The Restricted Boltzmann machine (RBM) is critical in the development of deep belief networks, which are considered the basis of deep learning. RBM is a bipartite graph that can be represented as an undirected or bidirectional graphical model with two layers [28]. It has two layers: a visible layer (vv) and a hidden layer (hh). The layers are connected using symmetrically weighted connections. The term "restricted" refers to the absence of visible-visible or hidden-hidden connections between neurons in a given layer. The figure depicts a constrained belief network with 4 visible nodes and 3 hidden nodes. Unlike the Boltzmann network, RBM does not influence on nodes within a single layer [29]. Restricted Boltzmann Machine is an unsupervised learning method that has the

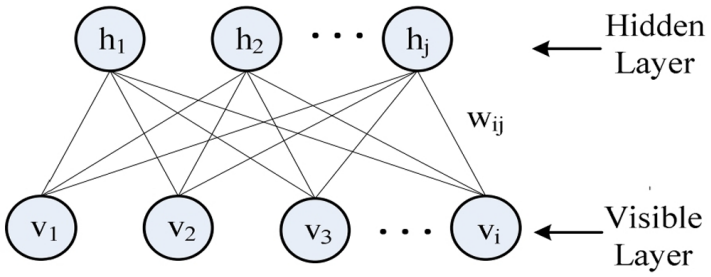

Figure 3.10 – An RBM with binary hidden units representing latent features and visibleunits encoding observed data

advantage of fitting the features of the samples. So, when we obtain an output from the hidden layer, we may use it as the visible layer's input to another RBM. This technique can be thought of as an additional feature extraction from the extracted features of our samples. Two forms of RBM are commonly used in DNN training. The two categories differ according to the input data values. First, suppose that both visible and buried units are binary 0 or 1. Binary units are represented using the Bernoulli distribution. RBM is

designed for binary hidden units and linear input with Gaussian noise. This RBM works with real-valued data [28].

3.3.2.3 Deep Belief Network (DBN

A Deep Belief Network (DBN) is a type of deep neural network that includes multilayer belief networks. DBN is a theoretical tool that is used to train and initialize several layers in deep neural networks. DBN is one of the most reliable deep learning algorithms, with great accuracy and computational efficiency [30]. DBN is a probabilistic, undirected vector graph model with stochastic variables [27]. DBN is an unsupervised learning method that reconstructs inputs from learned outputs [28]. DBN contains Restricted Boltzmann Machines (RBM) that are trained greedily. Each RBM layer communicates with the preceding and next levels [31] [32]. According to the figure, this model comprises a feedforward network and multiple layers of RBM as feature extractors [33]. RBM consists of only two layers: hidden and visible [34]. The building method is stack-wise and bottom-up. Each stack consists of two layers learned using RBM. Following each stack's training, the RBM's hidden layer is used as an observable layer to train the RBM in the following stack for a deeper hidden layer. Following this approach, we eventually train a bottom-up deep machine using a stack-wise and tandem-based training algorithm. DBN has been effectively applied to several tasks, such as handwriting recognition , speech recognition [35][36], audio classification [37], and text classification [38].

3.3.2.4 Deep Autoencoder

The auto-encoder, or auto-associator, is a common building block in deep neural networks. It consists of two modules: • An encoder uses a deterministic mapping function,

$$f : h = f(x) \tag{3.4}$$

- A decoder uses another deterministic mapping function:

$$g : x = g(h) \tag{3.5}$$

The encoder and decoder settings may be learned for real-valued input by reducing. The

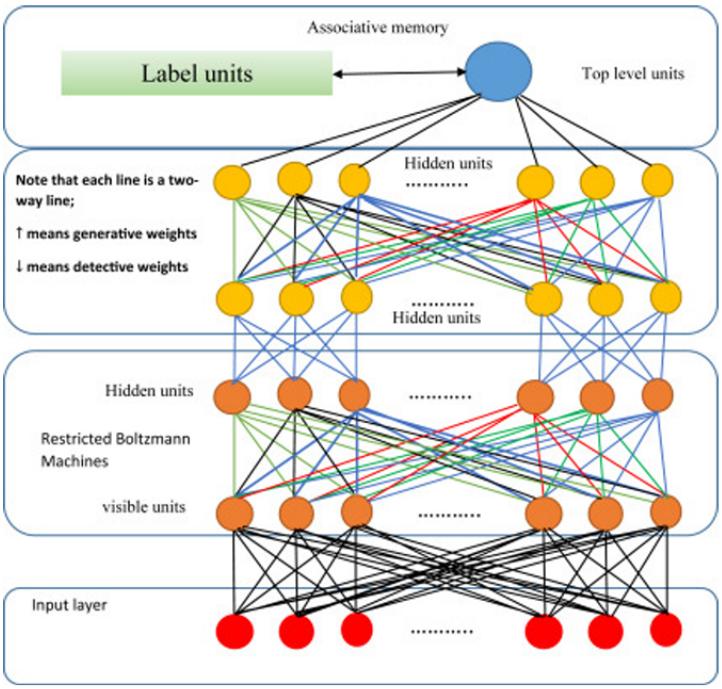

Figure 3.11 – The several layers of neural networks DBN

reconstruction error:

$$e = xg(f(x)) \tag{3.6}$$

The hidden layer's output is then used as a feature in picture representation. It has been established that this type of nonlinear autoencoder varies from PCA [39]. "Training an auto-encoder to minimize reconstruction error equates to maximizing a lower constraint on the mutual information between input and the learned representation," according to a single research study [40] Vincent et al. propose a denoising autoencoder that increases generalization by training on locally distorted inputs, hence improving autoencoder capabilities for image representation in deep networks. A deep auto-encoder is made up of two symmetrical deep-belief networks, each with four or five shallow levels representing the encoding half of the net and a second set of four or five layers representing the decoding half. The layers are limited Boltzmann machines, which are the fundamental components of deep-belief networks. The figure shows a simplified schema of a deep auto-encoder structure.

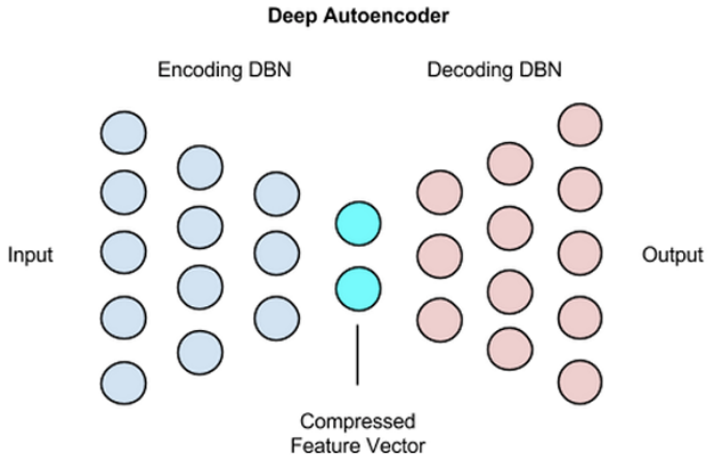

Figure 3.12 – The structure of deep auto-encoder.

3.3.2.5 Convolutional Neural Networks (CNN)

The convolutional neural network shown in Figure 3.13, Each CNN has two training stages: feed-forward and back-propagation. The usage of convolutional networks is a critical component of deep learning's effectiveness in image categorization [41]. A convolutional deep neural network (ConvNet) architecture [42][43] is made up of numerous trainable stages stacked on top of each other, followed by a supervised classifier. Each stage typically includes "three layers": a convolutional filter bank layer, a nonlinear processing layer, and a feature pooling layer. CNNs performed well in the field of activity recognition. This brings us back to the primary features of CNNs: local dependence and scale invariance. Local filters in CNN can detect local connections between neighboring sensor acceleration measures of an activity signal. Furthermore, CNN's scale invariance enables it to learn hidden characteristics from any position or size. This aids in the recognition of human actions because persons can perform the same activity at varying rates and intensities [44]. The convolution operation applies local filters to all subsets of the input, using shared weights. The pooling procedure divides the output features and applies functions to minimize the size of the previous layer, preserving scale invariance. This convolution produces feature maps that may identify various features at different temporal locations. The most prevalent CNN architectures are ZFNet [45], GoogLeNet [46], VGGNet [41], AlexNet [42], and ResNet [43].

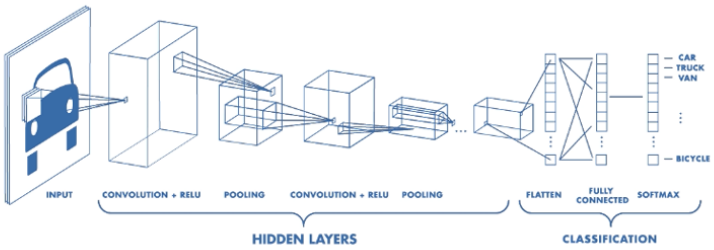

Figure 3.13 – A comprehensive guide to Convolutional Neural Networks (CNN)

3.3.2.6 AlexNet

Alexnet was created by Alex Krizhevsky and his collaborators in 2012. Although it has eight layers and learnable parameters, its design is similar to that of LeNet but more complex. The network accepts RBG pictures as input. This model consists of three fully connected layers with a Softmax classifier, five convolution layers, and max-pooling layers. They apply ReLU as an activation function. In addition, the network has two dropout layers [47].

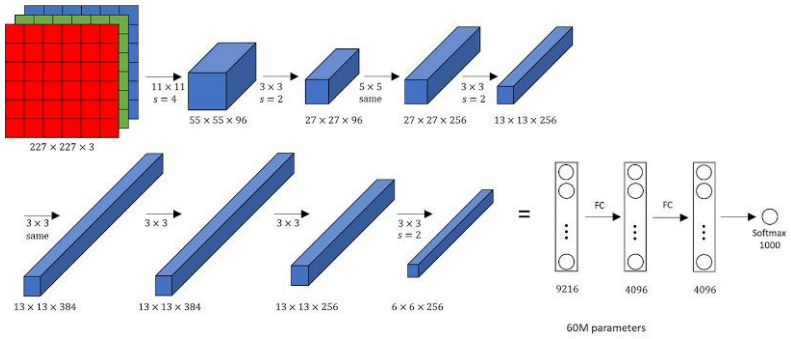

Figure 3.14 – Alexnet architecture

3.3.2.7 VGG 19

VGG-19, a pre-trained convolutional neural network, with 19 weight layers. The model is trained on millions of photos from the ImageNet dataset, representing around 10,000 different item categories. This VGG-19 design has 16 convolution layers, 3 fully linked layers, 5 max pool layers, and a softmax layer. The network extracts features from the input layer to the max pooling layer, and then uses the remaining features for classification. This work uses VGG-19 to extract characteristics from fingerprint photographs [48].

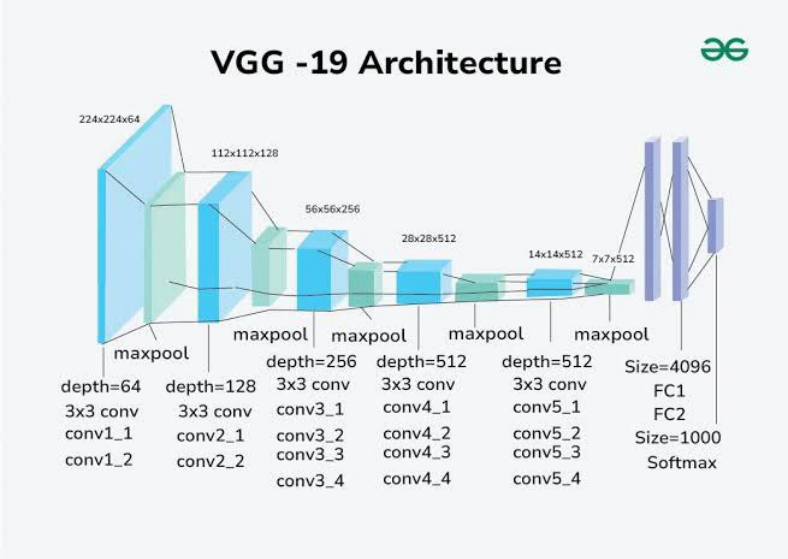

Figure 3.15 – vgg 19 architecture

3.3.2.8 ResNet 50

We employ ResNet-50 for deep feature extraction due to its minimal complexity and great performance. ResNet-50 is pre-trained on the ImageNet database and fine-tuned for PAD classification [49].

3.3.2.9 DenseNet

Huang et al. created DenseNet201, a convolutional neural network architecture, in 2017. The structure is highly linked, with each layer taking input from the previous layer and sending feature mappings to the next layer. This design improves information flow and mitigates the vanishing gradient problem. DenseNet201 is a parameter-efficient network that performs similarly to ResNet-101 but requires fewer parameters. Transition layers regulate complexity to optimize gradient flow, prevent overfitting, and increase model generalization.

3.4 Conclusion

Feature extraction is crucial for biometric systems in determining their accuracy, robustness, and adaptability. This chapter examined two major paradigms for encoding biometric data: hand-crafted and deep learning feature-based approaches, each with its own set of benefits and drawbacks.

Chapter 4

Results and discussions

4.1 Introduction

This chapter discusses the experimental results of unimodal and multimodal biometric identification systems that employ palm prints as biometric data. We used two pre-trained CNNs (AlexNet and Densenet201) and two hand-craft methods (LPQ and ML-LPQ) to extract and classify features from the dataset's images. The tests compared each network's performance on various palm pictures, measured improvement through consolidation at the resulting level, and evaluated the systems' overall performance. The objective is to develop reliable and efficient biometric identification systems that can handle the unpredictability and complexity of biometric data.

4.2 System Overview and Block Diagram

Our goal is to develop a multimodal biometric system using different sensors. Our study used CASIA datasets to determine the palm print class. For a multimodal biometric system, we will integrate it at the matching unit level after implementing the feature. Learning technology transfer is used to extract and classify single-mode systems (fine-tune) using AlexNet, DenseNet 201, and hand-crafted features LPQ and ML-LPQ (Figure 4.1).

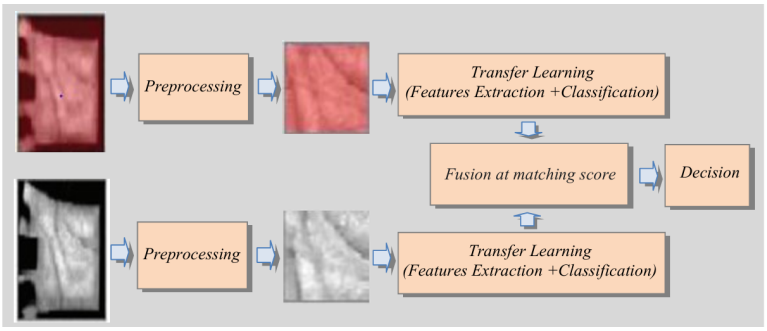

Figure 4.1 – Architecture of the identification system

4.3 Datasets used

CASIA's multispectral palmprint database contains 7,200 pictures of palmprint taken by 100 distinctive individuals employing a single multispectral imaging gadget planned by the company. All Palm images are 8-bit grayscale JPEG records. For each hand, we capture two palm image sessions. The time interval between the two sessions is more than a month. In each session, there are three tests. Each test contains six palm pictures that are captured at the same time with six distinctive electromagnetic spectra. The wavelengths of the illuminator compared to the six spectra are separately 460 nm, 630 nm, 700 nm, 850 nm, 940 nm, and white light. Between two tests, we permit a certain degree of variety within the stances of the hands. Much obliged to this, we point to extending the differing qualities of intra-class tests and reenacting common utilization.

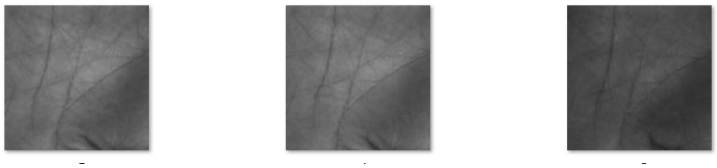

Figure 4.2 – Example palm print Images

4.4 Separation of Databases

The images used in our study consist of standard palmprint images. These photographs capture the normal designs and highlights on the palm. To partition the information, we embrace the taking-after methodology:

- **Training Images**: The training set consists of images captured during odd sessions. Specifically, images from sessions are utilized 2, 4, 6, 8, 10, and 12 for training.

- **Testing Images**: The testing set comprises images captured during even sessions. This includes images from sessions 1, 3, 5, 7, 9, and 11.

Utilizing this strategy, we guarantee that the system's execution is methodicallly assessed over a few sessions, which makes it less demanding to survey its exactness and capacity to recognize designs of palmprints.

4.5 Work environment

- **Hardware environment:**

- PC: DESKTOP-4HHIQN6
- Memory (RAM): 8.00 GB.
- Processor: Intel(R) Core(TM) i5-7300U CPU @ 2.60GHz 2.71 GHz.
- System type: 64-bit operating system.

- **Software environment:**

We have employed MATLAB R2021a as the logic tool in our method.

4.6 Experimental Results

4.6.1 Uni-modal biometric identification system

For a single-model biometric recognition system, we have established the equal error rate (EER) and the open group threshold (T_0). The recognition rate (ROR) and the order of the closed set of ideal recognition (RPR) were computed. After adjusting each pre-trained network (AlexNet, DenseNet201, LPQ) using the CNN model, the systems' performance was assessed using the predefined pattern. The outcomes for the indicator data set are displayed in the following table.

The evaluation highlights AlexNet's superior performance over DenseNet-201 across all metrics. AlexNet achieved the lowest error rate (ERR) of 0.1666, while DenseNet-201 showed higher error rates ranging from 0.8333 to 4.1666, with the 460 nm spectrum consistently yielding the lowest error values. Although threshold (T_0) values were similar between the two models, AlexNet demonstrated a higher recognition rate (ROR), ranging from 97.500 to 99.1667 across all spectrums, whereas DenseNet-201's ROR was notably lower, between 77.6667 and 95.833, performing well only in the 460 nm and WHT

Table 4.1 – Performance of uni-modal system for AlexNet and DenseNet 201 networks in the CASIA database.

Transfer Learning	Spectral bands	EER	T₀	ROR	RPR
AlexNet	460	0.1666	0.7473	99.1667	19
	630	0.1666	0.8085	98.5	5
	700	1.0000	0.6935	95.5	21
	850	0.5525	0.7293	96.667	11
	940	0.7094	0.7272	96	14
	WHT	0.1649	0.7319	98.667	5
DenseNet.201	460	0.8333	0.7273	95.833	12
	630	2.3334	0.688	86.3333	23
	700	3,1666	0.6830	82.833	94
	850	4.1666	0.6754	77.6667	80
	940	4.3197	0.6799	79.1667	71
	WHT	1.1667	0.6999	91.5	52

spectrums. Additionally, AlexNet required significantly fewer samples for recognition, as reflected in its superior performance ranking (RPR), further emphasizing its efficiency and accuracy compared to DenseNet-201.

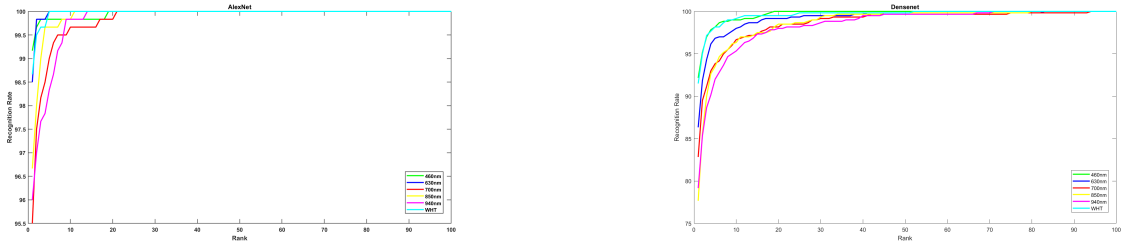

(a) 1 **(b)** 2

Figure 4.3 – Unimodal system performance: (a) AlexNet CMC curve, (b) CMC curve DenseNet 201.

Based on the results in Figure 4.3, in the first diagram (AlexNet), all wavelengths get good identification scores, with a minor variation between them. This is why it claimed "the results look almost the same"; even the 850 nm and 940 nm performed poorly, albeit less. The second graphic (DenseNet) clearly shows the difference between the wavelengths, and the less clear findings are notably obvious at 850 nm and 940 nm.

The analysis reveals that ML-LPQ outperforms standard LPQ across all evaluation metrics. The error rate (ERR) in ML-LPQ is minimal, ranging from 0.166 to 0.333 across all spectral bands, whereas standard LPQ shows significantly higher error rates,

Table 4.2 – Performance of a uni-modal system for LPQ and multi-level LPQ network in the CASIA database.

handcrafted features	Spectral bands	EER	T₀	ROR	RPR
LPQ	460	1.2448	0.7264	90.5	37
	630	2,9105	0.7034	83.3333	34
	700	4.5	0.6883	78.5	41
	850	4.1667	0.6877	76.1667	63
	940	4	0.6977	82.333	47
	WHT	2.0825	0.7044	88	51
Multi level LPQ	460	0.1666	0.6305	99.8333	24
	630	0.1667	0.7298	98.83333	17
	700	0.6666	0.6680	97	14
	850	0.1666	0.7385	99	3
	940	0.3333	0.676	98	43
	WHT	0.1947	0.6391	98.333	7

reaching up to 4. Despite the threshold (T_0) values being nearly identical in both methods, ML LPQ demonstrates a much higher recognition rate (ROR), peaking at 99 in the 850 nm spectrum. In comparison, standard LPQ achieves a maximum of only 90.5 in the 460 nm spectrum. Furthermore, ML-LPQ consistently surpasses LPQ in performance ranking (RPR), requiring fewer recognition attempts across all spectrums, highlighting its superior accuracy and efficiency.

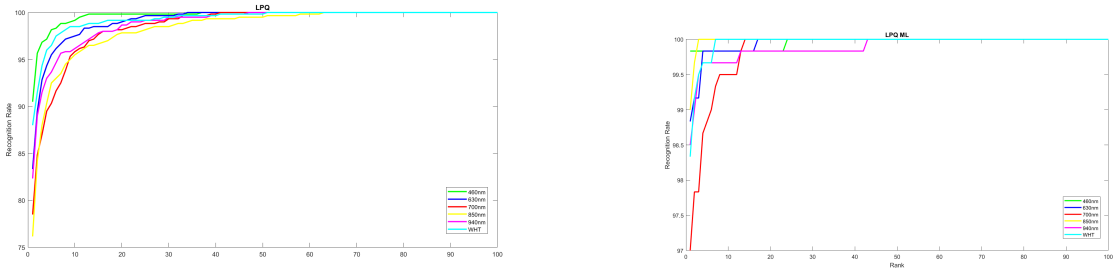

(a) **(b)**

Figure 4.4 – Unimodal system performance: (a) LPQ CMC curve, (b) CMC curve Multi-level LPQ.

Depending on the results, LPQ Wavelengths of 460 nm and 630 nm provide nearly comparable performance (high recognition rate). Lengths 850 nm and 940 nm perform poorly, and in LPQ, multi-level enhanced performance across all wavelengths and increased stability at higher ratios. Lengths 850 nm and 940 nm are still the least used. However, they have improved over standard LPQ.

Deep networks are the best choice for applications that demand great accuracy and consistency of outcomes, especially when there is enough data for training. Meanwhile, Multi-Level LPQ is an excellent choice if computational or data resources are constrained.

4.6.2 Multi-modal biometric identification system

Multimodal biometrics involves utilizing many biometric modalities to identify individuals. This technique can address constraints of unimodal biometric systems, including data noise, layer alterations, and layer similarities. Using a multimodal system aims to enhance system performance. The multimodal system achieves a low EER value, making it ideal for biometric identification.

We integrated the spectral bands in our multimodal system and conducted fusion experiments employing the basic sum rule (SUM) and the weighted sum rule (WHT SUM). Some spectra must be combined to improve system performance. We employ the CASIA database multimodality system to combine the database's six spectral bands one by one or between three spectral bands together. We considered two cases:

4.6.2.1 Case 01 - Fusion with the simple sum rule (SUM)

The simple sum rule, or SUM rule, is one of the simplest score-level fusion techniques in multi-source or multi-algorithm biometric identification systems.

Table 4.3 – Performance of a multimodal system for identification of AlexNet and DenseNet-201 networks in the CASIA database.

Transfer Learning	Spectral bands	EER	T_0	ROR	RPR
AlexNet	460 nm-630 nm	0.0101	0.888	99.6667	2
	700 nm-850 nm	0.000	0.935	99.8333	2
	940 nm-WHT	0.0135	0.921	99.5	2
	460 nm-630 nm-700 nm	0.000	0.847	100	1
	850 nm-940 nm-WHT	0.0235	0.884	99.333	2
DenseNet-201	460 nm-630 nm	0.3234	0.7719	97.3333	17
	700 nm-850 nm	1.0404	0.7272	91	79
	940 nm-WHT	0.4455	0.7676	96.5	21
	460 nm-630 nm-700 nm	0.4655	0.7398	79.5	55
	850 nm-940 nm-WHT	0.3430	0.7880	79	16

The performance comparison clearly shows AlexNet's superiority over DenseNet-201. AlexNet achieved the lowest EER values of 0.000 in the (700 nm-850 nm) and (460 nm-630

nm-700 nm) ranges, reflecting exceptional precision, and recorded a perfect recognition rate (ROR) of 100 in the (460 nm-630 nm-700 nm) range (Figure 4.5a). Its performance ranking (RPR) remained consistently low at 2 across all cases, indicating reliable and accurate recognition. In contrast, DenseNet-201 generally underperformed, with its highest EER of 1.0404 in the (700 nm-850 nm) range and the best ROR of 97.3333 in the (460 nm-630 nm) range. Its lowest EER was 0.3430 in the (850 nm-940 nm-WHT range, but the high RPR of 79 suggests that DenseNet-201 required significantly more ranking attempts to achieve accurate recognition, confirming its lower effectiveness compared to AlexNet (Figure 4.5b).

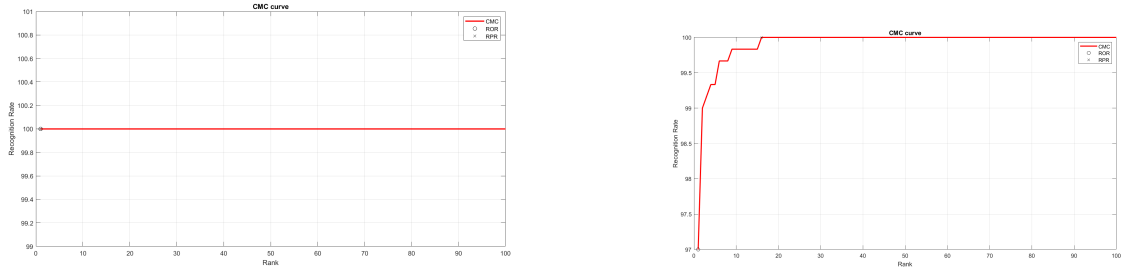

(a) **(b)**

Figure 4.5 – Multi-modal system performance (a) (460 nm-630 nm-700 nm) of the AlexNet CMC curve and (b) (850 nm-940 nm-WHT) DenseNet CMC curve.

The comparison between the two curves (Figure 4.5) highlights the superior performance of AlexNet over DenseNet-201. In the first curve, representing AlexNet, the red line remains flat at 100 across all ranks (1–100), indicating perfect classification where every test sample was correctly identified on the first attempt. In contrast, the second curve for DenseNet-201 starts at around 96 at Rank-1 and gradually improves, reaching 100 at approximately Rank-20. This reflects a more realistic scenario in which the model does not immediately recognize all samples but improves with higher ranks, demonstrating acceptable but less precise performance compared to AlexNet.

The evaluation demonstrates the superior performance of the Multi-level LPQ method over standard LPQ across all metrics. Multi-level LPQ achieved the lowest EER of 0.000 in the 460 nm-630 nm spectral range, indicating flawless classification, with other configurations also showing extremely low EER values, such as 0.0101. In contrast, LPQ recorded a much higher EER of 1.9747 in the 700 nm-850 nm range, reflecting poor relia-

Table 4.4 – Performance of a multimodal system for identification of LPQ and multilevel LPQ network in the CASIA database.

handcrafted features	Spectral bands	EER	T₀	ROR	RPR
LPQ	460 nm-630 nm	0.4653	0.7757	96	15
	700 nm-850 nm	1.9747	0.7128	90.1667	32
	940 nm-WHT	0.5	0.7628	95.833	27
	460 nm-630 nm-700 nm	0.5275	0.7731	96.8333	15
	850 nm-940 nm-WHT	0.5	0.751	96.6667	25
Multi level LPQ	460 nm-630 nm	0.000	0.939	99.833	2
	700 nm-850 nm	0.1649	0.6929	99.1667	4
	940 nm-WHT	0.0405	0.761	99.5	3
	460 nm-630 nm-700 nm	0.0101	0.886	99.6667	3
	850 nm-940 nm-WHT	0.0101	0.826	99.833	2

bility. Regarding threshold(T_0), Multi-level LPQ reached the highest value of 0.939 in the same optimal spectral band, confirming confident and accurate classification boundaries. In contrast, LPQ's thresholds were lower, notably 0.7128 in the 700-850 nm range. The recognition rate (ROR) for Multi-level LPQ exceeded 99 across all bands, with a peak of 99.833 in both the 460-630 nm and 850-940 nm-WHT ranges, whereas LPQ's ROR dropped to 90.1667 in the 700-850 nm band. Finally, Multi-level LPQ achieved an RPR as low as 2, showing high precision in early retrieval. At the same time, LPQ's RPR reached 32 in the worst case, highlighting a significant drop in ranking accuracy.

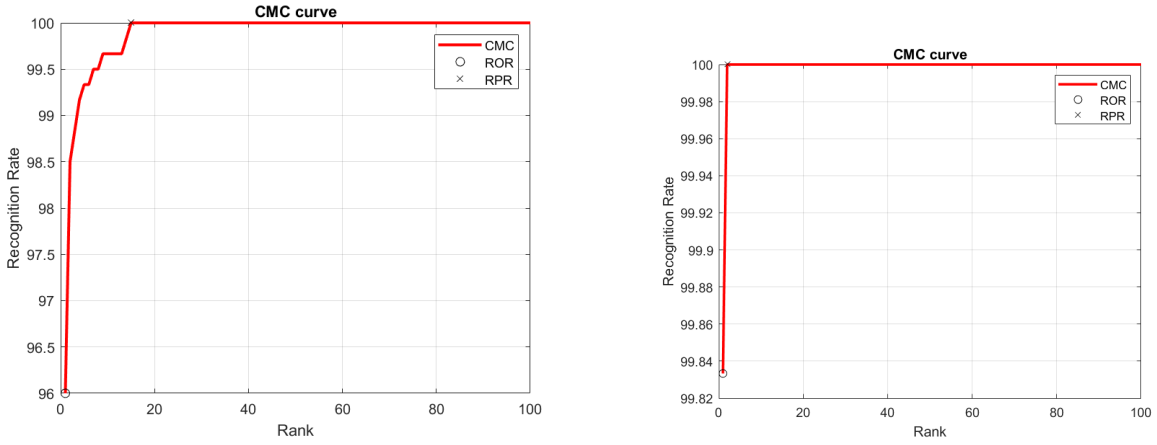

(a) **(b)**

Figure 4.6 – Multi-modal system performance: (a) (460 nm-630 nm) of LPQ CMC curve, (b) (460 nm-630 nm) multi-level LPQ CMC curve .

The first CMC curve starts with a recognition rate of about 96 at rank 1. It gradually rises to 100 by rank 15, indicating strong performance though slightly lower than the

first example, with a more gradual increase suggesting that some samples require higher ranks for accurate recognition. The second curve shows a sharp increase from rank 1 to above 99.833, nearly reaching 100 by rank 2, reflecting excellent performance where over 99.833 samples are correctly identified on the first attempt. ROR and RPR values suggest the system uses multiple comparison or fusion methods, all of which achieve near-perfect accuracy.

4.6.2.2 Case 02 - the weighted sum rule (WHT SUM)

It is a core-level fusion technique used in multi-source biometric systems. Contrary to the rule of simple addition (SUM), which treats all systems equally, WHT SUM weights each system or algorithm according to its importance or accuracy.

Table 4.5 – Performance of a multimodal system for identification of the AlexNet and DenseNet 201 networks of case 02 in the CASIA database.

Transfer Learning	Spectral bands	EER	T_0	ROR	RPR
AlexNet	460 nm-630 nm	0.0101	0.888	99.6667	2
	700 nm-850 nm	0.1749	0.7650	98	7
	940 nm-WHT	0.0437	0.8262	99.5	2
	460 nm-630 nm-700 nm	0.004	0.935	99.8333	2
	850 nm-940 nm-WHT	0.005	0.944	99.6667	2
DenseNet.201	460 nm-630 nm	0.3333	0.773	94.8333	16
	700 nm-850 nm	1.3334	0.7117	90.5	86
	940 nm-WHT	0.8058	0.7068	94	17
	460 nm-630 nm-700 nm	0.3097	0.7678	96.6667	11
	850 nm-940 nm-WHT	0.4577	0.7307	96.5	12

The analysis shows that AlexNet consistently outperforms DenseNet-201 across all evaluation metrics. It achieved the lowest EER value of 0.005 and the highest threshold (T_0) of 0.944 using the (850 nm-940 nm-WHT) range, indicating excellent classification accuracy and strong decision boundaries. In terms of recognition rate (ROR), AlexNet's best performance was 99.8333 in the (460 nm-630 nm-700 nm) domain, with all other domains also exceeding 99, while DenseNet-201's highest ROR was 96.5 in the same spectral range, indicating lower effectiveness. Moreover, AlexNet held the top performance ranking (RPR = 1), especially in the (460 nm-630 nm-700 nm) range, while DenseNet-201 recorded the lowest ranking score of 86 in the (700 nm-850 nm) range, highlighting its

comparatively poor performance.

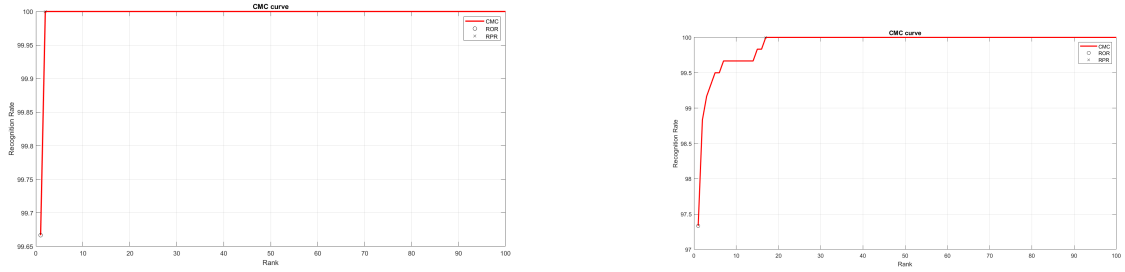

(a) **(b)**

Figure 4.7 – Multi-modal system performance (a) (460 nm-630 nm-700 nm)) of AlexNet CMC curve, (b) (460 nm-630 nm-700 nm)) DenseNet.201 CMC curve .

The first figure shows excellent performance, with the red CMC curve rising steeply and reaching nearly 100. This indicates that most correct identifications occurred at Rank-1, with a recognition rate of approximately 99.65. In contrast, the second figure starts lower at around 97.4 at Rank-1, and the curve gradually improves, reaching 100 by Rank 20. This suggests that while the method is still effective, it is less precise than the first, requiring higher ranks to achieve full recognition.

Table 4.6 – Performance of a multimodal system for identification of AlexNet and denseNet 201 network of the case 02 in the CASIA database.

handcrafted features	Spectral bands	EER	T_0	ROR	RPR
LPQ	460 nm-630 nm	0.4422	0.7827	95.6667	17
	700 nm-850 nm	1.8965	0.7153	90	32
	940 nm-WHT	0.8334	0.722	94.833	28
	460 nm-630 nm-700 nm	0.3894	0.7743	97.1697	18
	850 nm-940 nm-WHT	0.5	0.755	96.8333	28
Multi level LPQ	460 nm-630 nm	0.000	0.936	99.833	2
	700 nm-850 nm	0.1212	0.7155	99	4
	940 nm-WHT	0.0269	0.821	99.1667	3
	460 nm-630 nm-700 nm	0.000	0.943	99.8333	2
	850 nm-940 nm-WHT	0.006	0.88	99.833	2

The multi-level LPQ model demonstrated outstanding performance in terms of Equal Error Rate (EER), achieving the lowest EER value of 0.000 in the bands (460 nm–630 nm) and (460 nm–630 nm–700 nm). The highest EER recorded was 0.1212 in the (700 nm–850 nm) range, which is still relatively low. In contrast, the traditional LPQ technique performed poorly, with a maximum EER of 1.8965 in the same (700 nm–850 nm) range and

most values exceeding 0.3, indicating less accurate performance. Regarding the threshold (T_0), the multi-level LPQ showed high accuracy, with the highest T value of 0.949 in the (460 nm–630 nm–700 nm) range, whereas the standard LPQ experienced a significant drop, especially in the (940 nm–WHT) range, where the T_0 value was only 0.722. As for the recognition rate (ROR), the multi-level LPQ yielded impressive results, with nearly all values above 99 and the best ROR reaching 99.833 in the (460 nm-630 nm) range. In comparison, the LPQ's scores ranged from 90 to 97.1697, indicating lower performance. Finally, regarding RPR, the multi-level LPQ maintained a top performance across most bands (RPR = 2–4), while the traditional LPQ showed very poor performance, with the highest RPR reaching 32 in the (700 nm–850 nm) bands.

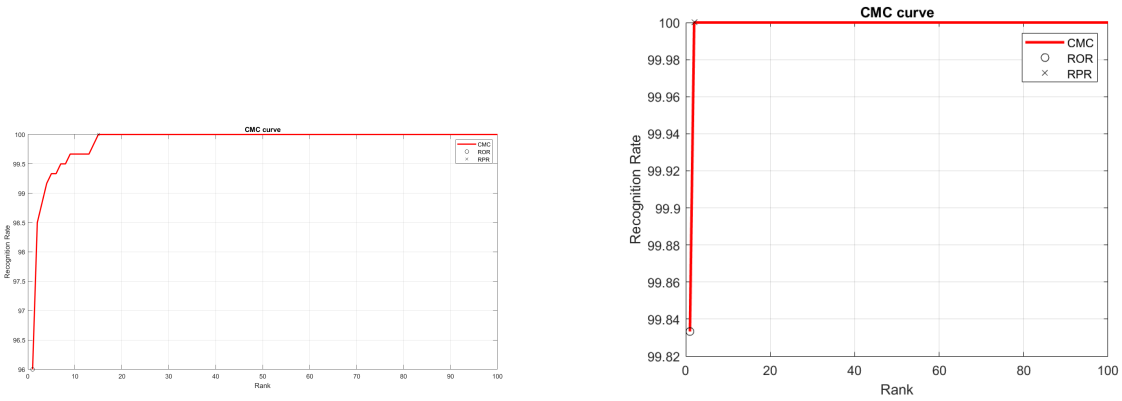

(a) **(b)**

Figure 4.8 – Multi-modal system performance (a) (460 nm-630 nm-700)) of LPQ CMC curve, (b)(460 nm-630 nm-700) Multi level LPQ CMC curve .

Figure 4.8a demonstrates average performance, with the CMC curve starting around 96 and reaching nearly 100 by rank 20. This indicates that some instances were not identified in the earliest ranks, but the overall performance remains satisfactory. In contrast, Figure 4.8b shows near-perfect performance, with the curve starting at 99.83 at rank 1 and achieving full accuracy by the second or third rank. This reflects the capabilities of a highly accurate and robust model in classification and identification tasks.

4.7 Conclusion

This chapter describes the development of a person identification system based on palm prints utilizing existing biometric research. We show how to develop a handprint recognition system using the LPQ, ML-LPQ, Alexnet, and Densenet algorithms for prop-

erty extraction. We found that the deep learning approach is the most efficient of the two proposed systems. The latter has also been upgraded with the addition of grades for a multi-pattern system. We saw a considerable and exceptional improvement in the identification rate after verifying these systems in databases (100%).

Chapter 5

General conclusion and future work

5.1 General conclusion

In recent years, palmprint has emerged as a reliable biometric means of identifying individuals due to its unique pattern and stability over time. In this thesis, we compared two major techniques for feature extraction in biometric systems: handcrafted features and deep learning-based features. The major goal was to compare the performance of both techniques in the context of biometric recognition, with palmprint pictures as the biometric modality.

For the handcraft technique, we used Local Phase Quantization (LPQ) and its version LPQ-ML, which are well-known for their resilience to light fluctuations and ability to capture local texture information effectively. These techniques performed well in terms of processing speed and cheap computational cost. However, its discriminative strength may be reduced when dealing with complicated or extremely comparable biometric patterns.

In contrast, we employed two pre-trained convolutional neural networks using the deep learning strategy: AlexNet and DenseNet-201. These models extracted deep features from photos, resulting in a more abstract and high-level representation of biometric data. The findings showed that deep features beat handcrafted features regarding recognition accuracy and generalization capabilities, especially when using Alexnet.

We also studied the characteristics of unimodal and multimodal biometric systems in terms of their structure, data sources used, and information processing layers. To improve the search results, we used different attribute extracts (descriptors) to extract properties from single—and multi-mode biometric systems. These methods have been analyzed to raise the recognition rate.

The quantitative comparison using the same dataset and assessment circumstances revealed that deep learning techniques outperform biometric recognition tasks. However, handcrafted features are still useful when computing economy and simplicity are important.

In summary, the decision between handcrafted and deep features should be based on

the unique needs of the target application. Deep learning models are more suited to high-accuracy and scalable systems, whereas handcrafted features may be preferred in low-resource contexts. In the future, it might be intriguing to investigate the integration of the visual transform model with augmentation in the database.

Bibliography

[1] S. K. Kihel, "Identification biométrique par fusion multimodale de l'empreinte d'articulation, l'empreinte digitale et l'empreinte veineuse du doigt," Ph.D. dissertation, Université Mohamed Boudiaf des sciences et de la technologie, 2017.

[2] M. Moulay and M. Arbaoui, "Authentification des personnes par l'articulation du doigt," Master's thesis, Université Kasdi Merbah Ouargla, 2015.

[3] D. Maltoni, D. Maio, A. K. Jain, and S. Prabhakar, *Handbook of Fingerprint Recognition*. Springer Science & Business Media, 2009.

[4] D. Zhang, W. K. Kong, J. You, and M. Wong, "Online palmprint identification," *IEEE Transactions on Pattern Analysis and Machine Intelligence*, vol. 25, no. 9, pp. 1041–1050, 2003.

[5] R. P. Wildes, "Iris recognition: an emerging biometric technology," *Proceedings of the IEEE*, vol. 85, no. 9, pp. 1348–1363, 1997.

[6] G. Betta, D. Capriglione, M. Corvino, C. Liguori, and A. Paolillo, "Face based recognition algorithms: A first step toward a metrological characterization," *IEEE Transactions on Instrumentation and Measurement*, vol. 62, no. 5, pp. 1008–1016, 2013.

[7] H. Matos, H. P. Oliveira, and F. Magalhães, "Hand-geometry based recognition system," in *Image Analysis and Recognition (ICIAR 2012)*, ser. Lecture Notes in Computer Science, A. Campilho and M. Kamel, Eds., vol. 7325. Springer, Berlin, Heidelberg, 2012.

[8] R. Joyce and G. Gupta, "Identity authorization based on keystroke latencies," *Communications of the ACM*, vol. 33, no. 2, pp. 168–176, 1990.

[9] "Communications of the acm," *Communications of the ACM*, vol. 43, no. 9, 2000.

[10] A. Karouni, B. Daya, and S. Bahlak, "Offline signature recognition using neural networks approach," *Procedia Computer Science*, vol. 3, pp. 155–161, 2011.

[11] G. Cui, L. Qin, Y. Wang, and X. Zhang, "An encryption scheme using dna technology," in *Bio-Inspired Computing: Theories and Applications, 2008. BICTA 2008. 3rd International Conference on.* IEEE, 2008, pp. 37–42.

[12] D. Bala, "Biometrics and information security," in *Proceedings of the 5th annual conference on Information security curriculum development.* ACM, 2008, pp. 64–66.

[13] A. K. Jain and A. Ross, "Information fusion in biometrics," *Pattern Recognition Letters*, vol. 24, pp. 2115–2125, 2003.

[14] J. L. Wayman, "Digital signal processing in biometric identification: a review," in *Proceeding of International Conference on Image Processing*, Rochester, NY, USA, 2002.

[15] M. El-abed, "Évaluation du systèmes biométriques," Thèse de doctorat, Université de Caen/Basse-Normandie, France, 2011.

[16] J. Malik *et al.*, "Reference threshold calculation for biometric authentication," *IJ Image, Graphics and Signal Processing*, vol. 2, pp. 46–53, 2014.

[17] S. G. Ababsa, "Authentification d'individus par reconnaissance de caractéristiques biométriques liées aux visages 2d/3d," Ph.D. dissertation, Evry-Val d'Essonne, 2008.

[18] Y. Du and C.-I. Chang, "Rethinking the effective assessment of biometric systems," *SPIE Newsroom*, pp. 1–3, 2007.

[19] M. El-Abed and C. Charrier, "Evaluation of biometric systems," in *New Trends and Developments in Biometrics*, 2012, pp. 149–169.

[20] T. Ojala, M. Pietikainen, and T. Maenpaa, "Multiresolution gray-scale and rotation invariant texture classification with local binary patterns," *IEEE Transactions on Pattern Analysis and Machine Intelligence*, vol. 24, no. 7, pp. 971–987, 2002.

[21] S. Brahnam, L. C. Jain, L. Nanni, A. Lumini *et al.*, *Local binary patterns: new variants and applications.* Springer, 2016.

[22] T. Ahonen, A. Hadid, and M. Pietikainen, "Face description with local binary patterns: Application to face recognition," *IEEE Transactions on Pattern Analysis and Machine Intelligence*, vol. 28, no. 12, pp. 2037–2041, 2006.

[23] V. Ojansivu and J. Heikkil"a, "Blur insensitive texture classification using local phase quantization," in *International Conference on Image and Signal Processing*. Springer, 2008, pp. 236–243.

[24] A. Dhall, A. Asthana, R. Goecke, and T. Gedeon, "Emotion recognition using phog and lpq features," in *2011 IEEE International Conference on Automatic Face & Gesture Recognition (FG)*. IEEE, 2011, pp. 878–883.

[25] D. Paper, *TensorFlow 2.x in the Collaboratory Cloud: An Introduction to Deep Learning on Google's Cloud Service*. Apress, 2021.

[26] J. Schmidhuber, "Deep learning in neural networks: An overview," *Neural networks*, vol. 61, pp. 85–117, 2015.

[27] G. E. Hinton, S. Osindero, and Y.-W. Teh, "A fast learning algorithm for deep belief nets," *Neural computation*, vol. 18, no. 7, pp. 1527–1554, 2006.

[28] M. W. Mak and J.-T. Chien, *Machine learning for speaker recognition*. New York: Cambridge University Press, 2020.

[29] R. Salakhutdinov, A. Mnih, and G. Hinton, "Restricted boltzmann machines for collaborative filtering," in *Proceedings of the 24th international conference on Machine learning*, 2007, pp. 791–798.

[30] A. Mosavi, S. Ardabili, and A. Varkonyi-Koczy, "List of deep learning models," 2020, pp. 202–214.

[31] Q. Zhang, Y. Xiao, W. Dai, J. Suo, C. Wang, J. Shi, and H. Zheng, "Deep learning based classification of breast tumors with shear-wave elastography," *Ultrasonics*, vol. 72, pp. 150–157, 2016.

[32] D. Wulsin, J. Gupta, R. Mani, J. Blanco, and B. Litt, "Modeling electroencephalography waveforms with semi-supervised deep belief nets: fast classification and anomaly measurement," *Journal of neural engineering*, vol. 8, no. 3, p. 036015, 2011.

[33] J. Patterson and A. Gibson, *Deep Learning: A Practitioner's Approach*. O'Reilly Media, Inc., 2017.

[34] S. Vieira, W. H. Pinaya, and A. Mechelli, "Using deep learning to investigate the neuroimaging correlates of psychiatric and neurological disorders: Methods and applications," *Neuroscience Biobehavioral Reviews*, vol. 74, pp. 58–75, 2017.

[35] A.-r. Mohamed, D. Yu, and L. Deng, "Investigation of full-sequence training of deep belief networks for speech recognition," in *Eleventh Annual Conference of the International Speech Communication Association*. Citeseer, 2010.

[36] C. Huang, W. Gong, W. Fu, and D. Feng, "A research of speech emotion recognition based on deep belief network and svm," *Mathematical Problems in Engineering*, vol. 2014, 2014.

[37] H. Lee, P. Pham, Y. Largman, and A. Ng, "Unsupervised feature learning for audio classification using convolutional deep belief networks," in *Advances in neural information processing systems*, vol. 22, 2009.

[38] T. Liu, "A novel text classification approach based on deep belief network," in *International Conference on Neural Information Processing*. Springer, 2010, pp. 314–321.

[39] N. Japkowicz, S. J. Hanson, and M. A. Gluck, "Nonlinear autoassociation is not equivalent to pca," *Neural Computation*, vol. 12, no. 3, pp. 531–545, 2000.

[40] P. Vincent, H. Larochelle, I. Lajoie, Y. Bengio, P.-A. Manzagol, and L. Bottou, "Stacked denoising autoencoders: Learning useful representations in a deep network with a local denoising criterion," *Journal of Machine Learning Research*, vol. 11, no. 12, 2010.

[41] L. Sifre and S. Mallat, "Rotation, scaling and deformation invariant scattering for texture discrimination," in *Proceedings of the IEEE Conference on Computer Vision and Pattern Recognition*, 2013, pp. 1233–1240.

[42] I. Goodfellow, D. Warde-Farley, M. Mirza, A. Courville, and Y. Bengio, "Maxout networks," in *International Conference on Machine Learning*. PMLR, 2013, pp. 1319–1327.

[43] K. Jarrett, K. Kavukcuoglu, M. Ranzato, and Y. LeCun, "What is the best multi-stage architecture for object recognition?" in *2009 IEEE 12th International Conference on Computer Vision*. IEEE, 2009, pp. 2146–2153.

[44] M. Zeng, L. T. Nguyen, B. Yu, O. J. Mengshoel, J. Zhu, P. Wu, and J. Zhang, "Convolutional neural networks for human activity recognition using mobile sensors," in *6th International Conference on Mobile Computing, Applications and Services*. IEEE, 2014, pp. 197–205.

[45] T.-h. Chan, K. Jia, S. Gao, J. Lu *et al.*, "Pcanet: A simple deep learning baseline for image classification?" *arXiv preprint arXiv:1404.3606*, 2014.

[46] Y. Zhou, W. Wang, and X. Huang, "Fpga design for pcanet deep learning network," in *2015 IEEE 23rd Annual International Symposium on Field-Programmable Custom Computing Machines*. IEEE, 2015, pp. 232–232.

[47] A. Krizhevsky, I. Sutskever, and G. E. Hinton, "Imagenet classification with deep convolutional neural networks," in *Advances in Neural Information Processing Systems*, vol. 25, 2012.

[48] K. Simonyan and A. Zisserman, "Very deep convolutional networks for large-scale image recognition," in *Proceedings of the 3rd International Conference on Learning Representations (ICLR)*, Y. Bengio and Y. LeCun, Eds., San Diego, CA, USA, 2015.

[49] K. He, X. Zhang, S. Ren, and J. Sun, "Deep residual learning for image recognition," in *Proceedings of the IEEE Conference on Computer Vision and Pattern Recognition (CVPR)*. Las Vegas, NV, USA: IEEE, 2016, pp. 770–778.